ELSEVIER
Sensors and Actuators 82 (2000) 274–280
SENSORS ACTUATORS A PHYSICAL
www.elsevier.nl/locate/sna

Fracture toughness of polysilicon MEMS devices

H. Kahn [a,*], N. Tayebi [b], R. Ballarini [c], R.L. Mullen [c], A.H. Heuer [a]

[a] Department of Materials Science and Engineering, Case Western Reserve University, 10900 Euclid Avenue, Cleveland, OH 44106-7204, USA
[b] Department of Mechanical and Aerospace Engineering, Case Western Reserve University, 10900 Euclid Avenue, Cleveland, OH 44106-7222, USA
[c] Department of Civil Engineering, Case Western Reserve University, 10900 Euclid Avenue, Cleveland, OH 44106-7201, USA

Received 7 June 1999; received in revised form 9 November 1999; accepted 10 November 1999

Abstract

Polysilicon fracture mechanics specimens have been fabricated using standard microelectro-mechanical systems (MEMS) processing techniques, with characteristic dimensions comparable to typical MEMS devices. These specimens are fully integrated with simultaneously fabricated electrostatic actuators that are capable of providing sufficient force to ensure catastrophic crack propagation. Thus, the entire fracture experiment takes place on-chip, eliminating the difficulties associated with attaching the specimen to an external loading source. The specimens incorporate atomically sharp cracks created by indentation, and fracture is initiated using monotonic electrostatic loading. The fracture toughness values are determined using finite element analysis (FEA) of the experimental data, and show a median value of 1.1 MPa $m^{1/2}$. © 2000 Elsevier Science S.A. All rights reserved.

Keywords: Microelectromechanical systems; Polysilicon; Fracture toughness; Surface micromachining

1. Introduction

Numerous microelectro-mechanical systems (MEMS) devices have been developed which use polysilicon as the major structural material [1]. For applications where large movements are desirable, it is advantageous to design for deflections that correspond to a safe fraction of the polysilicon strain limits. However, the relevant material properties, such as fracture toughness, are not well characterized for polysilicon at these size scales, or for polysilicon which has been subjected to MEMS fabrication techniques.

There have been a few recent reports on the fracture toughness of polysilicon MEMS test specimens which contained micromachined notches. Sharpe et al. [2] and Tsuchiya et al. [3] employed external piezoelectric load cells to fracture their notched specimens, and reported critical stress intensity factors, K_{Ic}, of 1.4 and 1.9 to 4.5 MPa $m^{1/2}$, respectively. These are associated with finite radius (1.0 and 0.23 μm, respectively) notches and thus do not represent true fracture toughness. The present authors have previously reported J_c (critical energy release rates determined using the J-integral) values of 16 to 62 N/m for externally wedge-loaded specimens [4] and 63 ± 20 N/m for electrostatically loaded specimens [5]; the nominal fracture toughness of the latter specimens is 3.5 MPa $m^{1/2}$ [6], and all specimens included 1.0 μm radius notches. Fractographic investigations of the electrostatically fractured polysilicon specimens can be used to determine the initial flaw size and indicate toughness values of 1 to 2 MPa $m^{1/2}$ [5]. All of these values are higher than those accepted for single crystal silicon ($K_{Ic} \sim 0.9$ MPa $m^{1/2}$; $J_c \sim 4.8$ N/m [4]), as well as for the reported values for bulk polysilicon (K_{Ic} 0.75 to 0.87 MPa $m^{1/2}$) [7,8]; in those latter tests, however, the polysilicon grain size was quite large, ~ 1 mm, and thus much larger than the flaw size, which is typically not the case for MEMS structures.

The use of micromachined notches to create the stress concentrations necessary for fracture has two distinct shortcomings. Firstly, there simply is no singularity; therefore K, the stress intensity, cannot be specified in the conventional manner, and the experimental results cannot be directly related to K_{Ic}. In fact, a study of the effect of notch radius on the fracture of single crystal silicon along the {111} plane reported nominal K_{Ic} values that varied from 1.24 to 2.85 MPa $m^{1/2}$ for radii of 80 to 580 μm [9]. Secondly, the morphology of the etched surface, namely the smoothness of the sidewalls on the inside of the notch, will play an important role in the fracture behavior. There-

* Corresponding author. Tel.: +1-216-368-6499; fax: +1-216-368-3209.
E-mail address: hxk29@cwru.edu (H. Kahn).

0924-4247/00/$ - see front matter © 2000 Elsevier Science S.A. All rights reserved.
PII: S0924-4247(99)00366-0

GE-1027.001

DOCKET ALARM
Find authenticated court documents without watermarks at docketalarm.com.

fore, the measured fracture properties will display a dependence on the etching technique and will not be inherent materials properties.

The present work involves micromachined fracture mechanics specimens that were integrated with electrostatic actuators that contain either 1456 or 1658 pairs of interdigitated comb fingers. The specimens include atomically sharp cracks created by indentation, which eliminates the complications involved with micromachined notches. To the present authors' knowledge, this experiment is the first to report the fracture toughness of a MEMS material using an atomically sharp crack. (Strictly speaking, as discussed below, the crack tip may not be ''atomically'' sharp, but may be a few atomic spacings in radius.) The integrated electrostatic actuator allows the entire experiment to take place on-chip without any external-loading source. Another advantage is the possibility of resonating the actuator in order to achieve cyclic loading at very high frequencies (the resonance frequencies of the actuators are ~ 20 kHz), in order to study fatigue behavior conveniently.

2. Experiment

2.1. Device fabrication

A completed device is shown in the scanning electron micrograph (SEM) in Fig. 1a, with a magnified image of the fracture mechanics specimen in Fig. 1b, a higher magnification view of the initial crack in Fig. 1c, and a view of the specimen after fracture in Fig. 1d. The left side of the fracture mechanics specimen, as oriented in Fig. 1b, is fully released (courtesy of the release holes visible in the micrograph) and is free to move, while the right side is anchored to the substrate. When a voltage is applied to the comb fingers of the actuator, it will pull the left side of the fracture mechanics specimen downward, creating a stress concentration at the crack tip. A sufficient voltage will cause enough displacement in the end of the specimen to establish a critical stress intensity, K_{Ic}, and catastrophic propagation of the crack.

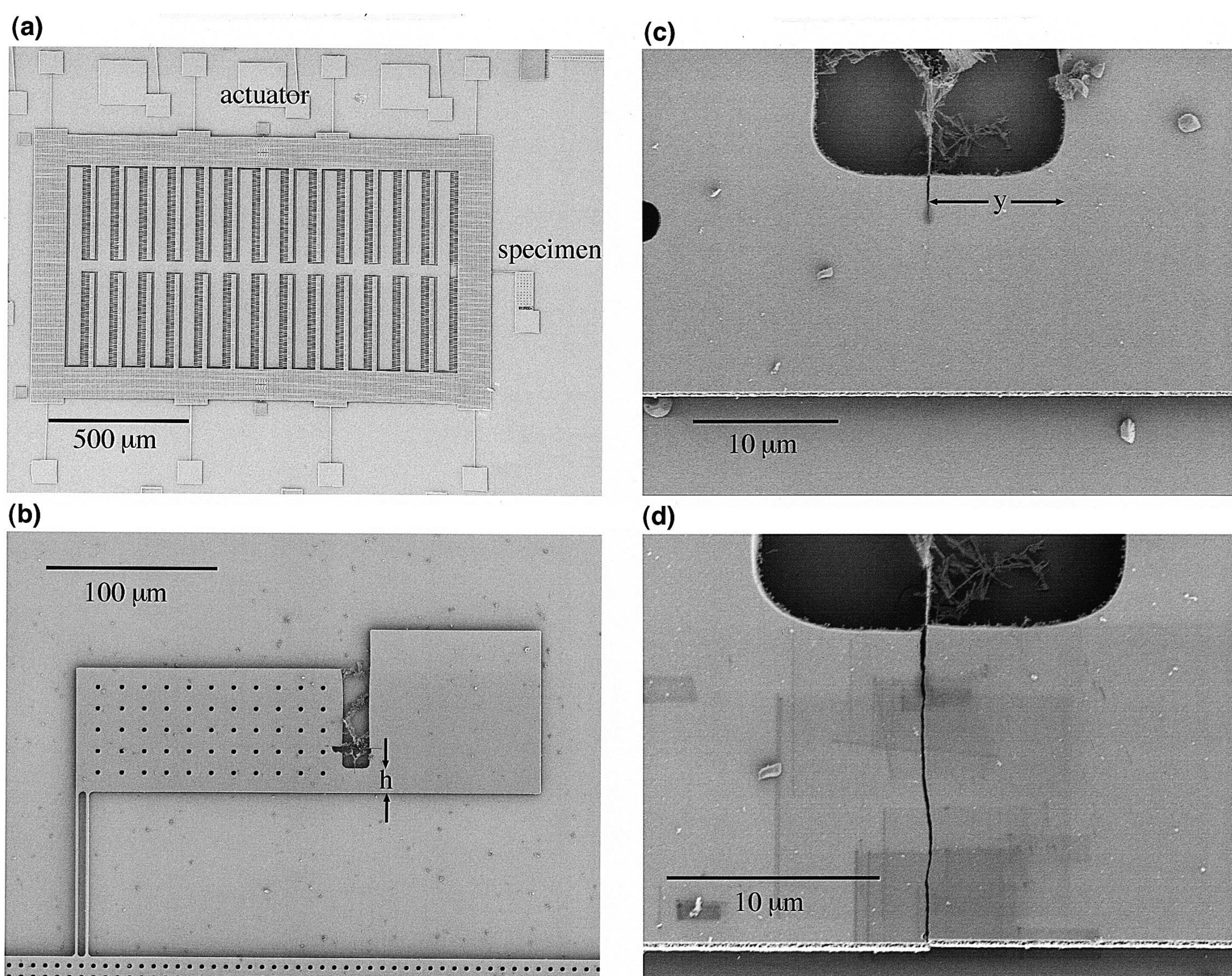

Fig. 1. SEM micrographs of (a) MEMS fracture device showing integrated actuator and fracture mechanics specimen, (b) magnified (and rotated 90°) view of fracture mechanics specimen (h indicates the beam depth), (c) magnified view of the specimen ligament showing the initial crack, (d) specimen ligament following the fracture experiment (y indicates the distance from the initial crack to the fixed end of the specimen).

GE-1027.002

DOCKET ALARM Find authenticated court documents without watermarks at docketalarm.com.

The devices were fabricated in a two-mask process, illustrated in Fig. 2 and summarized, as follows. The release oxide (3.0 μm) was thermally grown, the polysilicon (3.5 μm) was deposited by LPCVD at 580°C, followed by an anneal at 1000°C for 1 h in nitrogen, and the masking oxide (1.0 μm) was deposited by LPCVD at 450°C (Fig. 2a). The masking oxide was photolithographically patterned and was dry etched using CHF_3/C_2F_6, and the polysilicon was dry etched using Cl_2 (Fig. 2b). At this point a Vickers indent (with a 200-g load) was placed on the specimen, causing radial cracks to form at the indent corners (Fig. 2c); an example is shown in Fig. 3. The wafer was then annealed at 1000°C for 30 min (in air) to relieve the residual stresses induced by indentation; otherwise, the portion of the specimen surrounding the indent often de-laminated from the substrate during further processing, as shown in Fig. 4. Presumably, the de-lamination is due to lateral cracks and high residual stresses induced by indentation. A lateral crack beneath the indent can be seen in the infrared microscope image in Fig. 5a; the lateral crack remains after annealing (Fig. 5b), but the reduced residual stresses do not provide sufficient driving force for the lateral crack to propagate. Following this anneal, a second photolithographic mask protected the majority of the device, allowing the indent and its related damage to be etched away (using Cl_2), while the radial cracks remained in the specimen (Fig. 2d). The devices were then time-released in HF, followed by supercritical CO_2 drying (Fig. 2e). (This technique for forming sharp cracks in micromachined MEMS specimens was first proposed by Keller [10], though no fracture results were reported; it is commonly employed in studying bulk ceramics.) The residual stress of the released polysilicon was measured with an on-chip micro-strain gauge [5] to be 12 ± 5 MPa. For sufficient conductivity for electrostatic actuation, the devices were sputter-coated with ~ 10 nm of palladium following release.

A problem with performing photolithography on a substrate that contains cracks is that it is very difficult to remove any photoresist that enters the cracks. Therefore, in subsequent etching steps, some areas where the cracks had been will be unintentionally masked. In these devices, this causes debris to be present, which can be seen just above the initial crack in Fig. 1b, c and d. However, this extra material, which is polysilicon, is mostly unattached to the specimen and does not interfere with its movement. It is not believed to affect the experimental measurements.

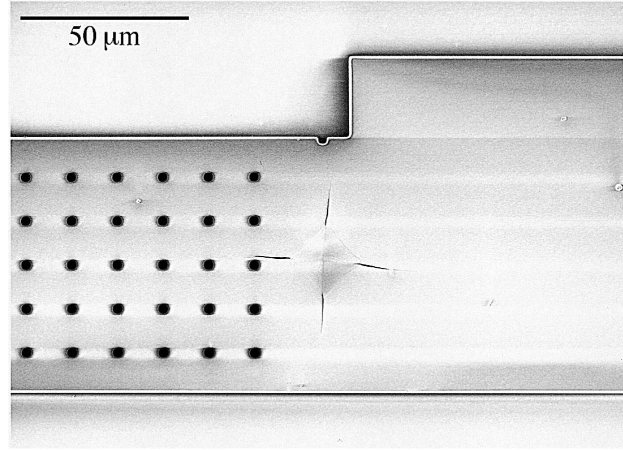

Fig. 3. SEM micrograph of an indented specimen, before the second polysilicon etch.

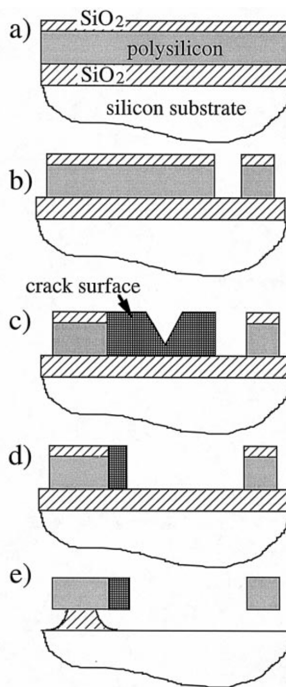

Fig. 2. Schematic drawings showing the fabrication sequence of the devices.

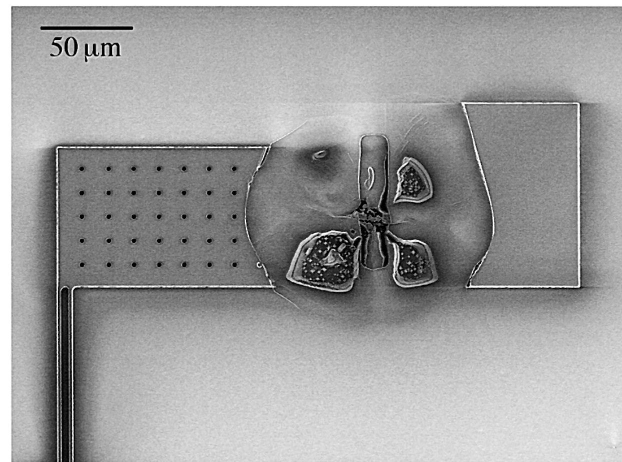

Fig. 4. SEM micrograph of a specimen which was not annealed following indentation and suffered de-lamination.

GE-1027.003

DOCKET ALARM
Find authenticated court documents without watermarks at docketalarm.com.

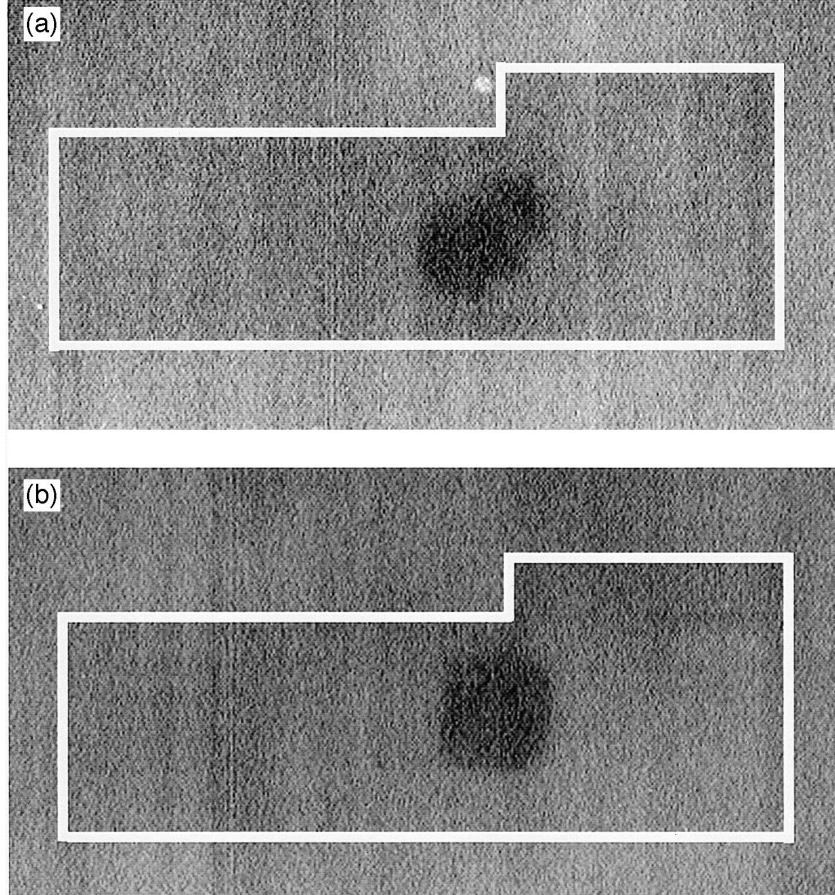

Fig. 5. Infrared microscope images of indented specimens before the second polysilicon etch, (a) before annealing and (b) after annealing. Because of the poor contrast of the images, the specimens are artificially outlined in white, as a visual aid.

2.2. *Experimental procedure*

The initial crack lengths and positions for all of the fracture mechanics specimens were measured using an SEM before testing. The devices were tested using DC electrostatic actuation. The applied voltage was increased until the crack propagated catastrophically, at which point the voltage at fracture could be recorded directly from the power supply. A micrograph of a specimen after testing is shown in Fig. 1d. During the test, the displacement of the actuator was recorded. For half the experiments, the critical actuator displacements were measured visually using an optical microscope with an accuracy of 0.3 μm. For the other half, the experiments were recorded on video tape using the same optical microscope, and the appropriate images were digitally captured and analyzed to determine the critical displacements with an accuracy of 0.15 μm.

The critical voltage at fracture could be measured much more accurately than the displacements, and so the first attempt to determine the forces being applied to the specimens was to develop an accurate voltage versus force calibration for the actuators [11]. However, the actuator displacement versus voltage behavior did not correlate well from device to device. The most likely explanation is that varying amounts of debris can accumulate underneath the actuators (they are quite large), either during release or during subsequent handling in the non-clean room laboratory environment. Therefore, the displacements of the actuators, i.e., the displacements of the free ends of the fracture mechanics specimens, were used in conjunction with finite element analysis (FEA) of the structure, using the FRANC2D simulation program [12], to determine the critical stress intensity. The crack was assumed to propagate catastrophically with no increase in the initial crack length, and the actual dimensions of the anchor (including the undercutting that occurred during release) were included in the model. The error in the FEA calculations was determined to be on the order of a few percent by comparison with handbook solutions.

3. Results and discussion

Three different fracture mechanics specimen designs were tested. They differed only in the depth of the beam (labeled h in Fig. 1b), which was 10, 15 or 20 μm. Due to the stochastic nature of the crack paths created by indentation, the initial crack lengths varied a great deal. In

GE-1027.004

DOCKET ALARM Find authenticated court documents without watermarks at docketalarm.com.

Table 1
Experimental fracture toughness, K_{Ic}, data for polysilicon fracture mechanics specimens

Crack length a (μm)	Beam depth h (μm)	a/h (%)	Distance from crack to fixed end (μm)	Critical displacement (μm)	K_{Ic} (MPa $m^{1/2}$)	Experimental error in K_{Ic} (MPa $m^{1/2}$)
0.91	15	6	4.7	0.5	0.2	0.11
4.9	10	49	2.7	1.85	0.44	0.04
0.76	15	5	4.5	2.31	0.67	0.04
1.3	15	9	3.0	1.5	0.82	0.07
8.9	20	45	2.9	0.8	0.8	0.3
15	20	75	0.9	1.2	0.87	0.22
8.9	20	45	6.5	0.5	0.9	0.5
11	20	55	1.8	1.2	0.94	0.23
3.0	15	20	7.5	0.5	1.0	0.2
2.9	15	19	2.7	1.54	1.1	0.10
9.6	20	48	4.9	0.62	1.1	0.30
1.9	15	13	0.0	1.54	1.1	0.27
1.7	15	11	6.6	1.5	1.2	0.24
7.6	20	38	5.3	1.38	1.5	0.16
3.2	15	21	5.0	2.0	1.6	0.24
5.7	15	38	2.2	1.54	1.7	0.17
3.5	15	23	7.0	2.0	1.8	0.14
7.6	20	38	4.5	1.2	1.9	0.48
13	20	65	4.5	1.8	2.0	0.33
10	20	50	4.1	1.50	2.2	0.45

addition, the distance between the initial crack and the fixed end of the specimen (labeled y in Fig. 1c) was also variable. However, both of these factors were taken into account in the FEA, as well as any perpendicular cracks that remained in other parts of the specimen, as seen in Figs. 1b and 3. The experimental results are listed in Table 1, and the K_{Ic} values are plotted in Fig. 6, a Weibull plot [13]. The Weibull scale parameter, K_{Ic_o}, is 1.4 MPa $m^{1/2}$, and the Weibull modulus, m, is 1.9. (The straight line fit has a regression coefficient, R^2 of 0.94.) The Weibull distribution is commonly used to model fracture data and to predict failure statistics, but is not generally used for

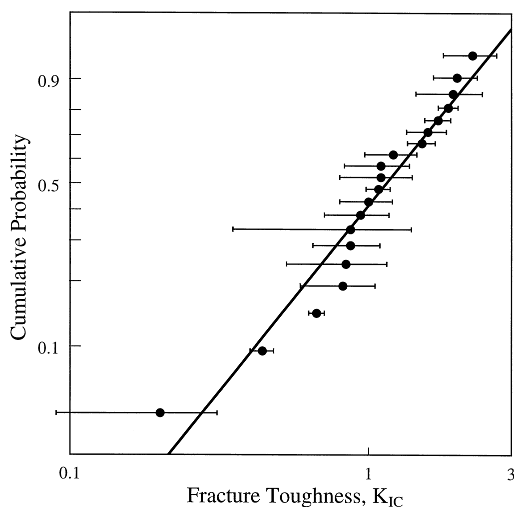

Fig. 6. Experimental fracture toughness, K_{Ic}, data for polysilicon fracture mechanics specimens.

fracture toughness, as K_{Ic} is assumed to be a material parameter. Its use here is simply a convenient way to describe the statistics of our determination of K_{Ic}.

The median K_{Ic} for polysilicon from our work is 1.1 MPa $m^{1/2}$. This value is lower than that determined by most notched polysilicon specimens reported previously [1–5], and is close to the values reported for single crystal silicon. The measured Weibull modulus is quite low, however, which indicates a large deviation in the values. (For good structural ceramics, the Weibull modulus is greater than 10.) As seen in Table 1, the K_{Ic} values do not correlate with the initial crack length, beam depth or critical displacement. Following the experiments, the released ends of the fracture mechanics specimens could be broken off, and the fracture surfaces examined. SEM micrographs of five different fracture surfaces (in the vicinity of the initial crack front) are shown in Fig. 7a, b, c, d and e, which correspond to K_{Ic} values of 0.4, 1.0, 1.2, 1.6 and 2.2, respectively. The initial crack front can be seen quite clearly, probably due to some modest blunting of the crack tip from dislocation emission during the 1000°C anneal following indentation [14]. The morphology of all the fracture surfaces in Fig. 7 appear quite similar and do not reveal an obvious source of the differences in K_{Ic}.

One possible source for the large deviation in K_{Ic} would be the effects of varying grain orientation near the crack tip. However, the grain size in these polysilicon films is very small (~0.1 μm), and the precrack passes through many grains. In addition, the effect of orientation on K_{Ic} in silicon is not large for the low index planes,

GE-1027.005

DOCKET ALARM
Find authenticated court documents without watermarks at docketalarm.com.

DOCKET ALARM

Explore Litigation Insights

Docket Alarm provides insights to develop a more informed litigation strategy and the peace of mind of knowing you're on top of things.

Real-Time Litigation Alerts

Keep your litigation team up-to-date with **real-time alerts** and advanced team management tools built for the enterprise, all while greatly reducing PACER spend.

Our comprehensive service means we can handle Federal, State, and Administrative courts across the country.

Advanced Docket Research

With over 230 million records, Docket Alarm's cloud-native docket research platform finds what other services can't. Coverage includes Federal, State, plus PTAB, TTAB, ITC and NLRB decisions, all in one place.

Identify arguments that have been successful in the past with full text, pinpoint searching. Link to case law cited within any court document via Fastcase.

Analytics At Your Fingertips

Learn what happened the last time a particular judge, opposing counsel or company faced cases similar to yours.

Advanced out-of-the-box PTAB and TTAB analytics are always at your fingertips.

API

Docket Alarm offers a powerful API (application programming interface) to developers that want to integrate case filings into their apps.

LAW FIRMS

Build custom dashboards for your attorneys and clients with live data direct from the court.

Automate many repetitive legal tasks like conflict checks, document management, and marketing.

FINANCIAL INSTITUTIONS

Litigation and bankruptcy checks for companies and debtors.

E-DISCOVERY AND LEGAL VENDORS

Sync your system to PACER to automate legal marketing.